

Proton Track Identification in MicroBooNE Simulation for Neutral Current Elastic Events

MICROBOONE-NOTE-1025-PUB

The MicroBooNE Collaboration

(Dated: January 25, 2017)

The net contribution of the strange quark spins to the proton spin, Δs , can be determined from neutral current elastic neutrino-proton interactions at low momentum transfer combined with data from electron-proton scattering. The probability of neutrino-proton interactions depends in part on the axial form factor, which represents the spin structure of the proton and can be separated into its quark flavor contributions. Low momentum transfer neutrino neutral current interactions can be measured in MicroBooNE, a high-resolution liquid argon time projection chamber (LArTPC) in its first year of running in the Booster Neutrino Beamline at Fermilab. The signal for these interactions in MicroBooNE is a single short proton track. We present our work on the automated reconstruction and classification of proton tracks in LArTPCs, an important step in the determination of neutrino-nucleon cross sections and the measurement of Δs .

I. INTRODUCTION

The structure of a nucleon is more interesting than the three familiar up and down valence quarks. These three quarks only account for a small percent of the nucleon mass. The gluons that bind the quarks split into quark-antiquark pairs of up, down, and strange flavor. The remainder of the nucleon mass is carried by this quark-gluon sea. The structure of the sea and how its elements combine with the valence quarks to give the nucleon its measured structure is not precisely known.

The net spin of the proton comes from a combination of the spin and orbital momentum of the quarks and gluons. The net contribution from the spin of strange quarks and antiquarks, Δs , is defined as

$$\Delta s = \int_0^1 \Delta s(x) dx$$

$$\Delta s(x) = \sum_{r=\pm 1} r[s^{(r)}(x) + \bar{s}^{(r)}(x)],$$

where $s(\bar{s})$ is the spin-dependent parton distribution function of the strange (anti)quark, r is the helicity of the quark relative to the proton helicity and x is the Bjorken scaling variable [1]. In the static quark model this value is zero.

In the 1980s the European Muon Collaboration [2] and several subsequent experiments found that the Ellis-Jaffe Sum Rule was violated in polarized, charged-lepton, inclusive, deep inelastic scattering (DIS). The Ellis-Jaffe sum rule [3] assumes that SU(3) flavor symmetry is valid and that $\Delta s = 0$. For the results to be consistent with exact SU(3) flavor symmetry, Δs must be *negative*. Follow-up measurements using semi-inclusive deep inelastic scattering have been consistent with $\Delta s = 0$, but these determinations of Δs are highly dependent on the fragmentation functions used [4].

An independent determination of Δs can be made using neutral-current (NC) elastic neutrino-proton scattering. The NC elastic cross section depends directly on

Δs and no assumptions about SU(3) flavor symmetry or fragmentation functions are needed.

II. ELASTIC NEUTRINO-PROTON SCATTERING

The elastic lepton-nucleon scattering cross section depends on the axial, electric, and magnetic form factors which represent the finite structure of the nucleon. The axial form factor, G_A , represents the spin structure, and the electric and magnetic form factors, G_E and G_M , represent the electric and magnetic structure, respectively.

A. Neutral-current elastic scattering

The NC elastic neutrino-proton cross section [1] can be written as

$$\begin{aligned} \left(\frac{d\sigma}{dQ^2}\right)_\nu^{NC} &= \frac{G_F^2}{2\pi} \left[\frac{1}{2} y^2 (G_M^{NC})^2 \right. \\ &+ \left(1 - y - \frac{M}{2E} y\right) \frac{(G_E^{NC})^2 + \frac{E}{2M} y (G_M^{NC})^2}{1 + \frac{E}{2M} y} \\ &+ \left(\frac{1}{2} y^2 + 1 - y + \frac{M}{2E} y\right) (G_A^{NC})^2 \\ &\left. + 2y \left(1 - \frac{1}{2} y\right) G_M^{NC} G_A^{NC} \right], \end{aligned}$$

where G_F is the Fermi constant, M is the mass of the nucleon, E is the neutrino energy, and Q^2 is the momentum transfer.

The neutral-current form factors, G_A^{NC} , G_E^{NC} , and G_M^{NC} , are functions of Q^2 and can all be written as a

linear combination of the individual quark contributions

$$\begin{aligned}
G_{E,M}^{NC,p}(Q^2) &= \left(1 - \frac{8}{3}\sin^2\theta_W\right) G_{E,M}^u(Q^2) \\
&+ \left(-1 + \frac{4}{3}\sin^2\theta_W\right) G_{E,M}^d(Q^2) \\
&+ \left(-1 + \frac{4}{3}\sin^2\theta_W\right) G_{E,M}^s(Q^2) \\
G_A^{NC,p}(Q^2) &= \frac{1}{2} [-G_A^u(Q^2) + G_A^d(Q^2) + G_A^s(Q^2)].
\end{aligned}$$

The up, down, and strange quark contributions to the electric and magnetic form factors of the proton have been determined in a world-wide measurement program of elastic electron-proton scattering using hydrogen targets and quasi-elastic electron-nucleon scattering using light nuclear targets (specifically deuterium and helium) [5, 6].

We plan to measure the ratio of the neutral-current elastic cross section to the charged-current elastic cross section. The charged-current (CC) elastic cross section does not depend on Δs , but it is better known than the NC elastic cross section. Taking the ratio of the two cross sections reduces systematic uncertainty on our measurement due to the beam flux, detector efficiency, and nuclear effects and final state interactions in argon nuclei.

B. Axial form factor

At the limit when the momentum transfer (Q^2) goes to zero, the quark contributions to the axial form factor become the net contribution of individual quark spin to the proton spin,

$$G_A^q(Q^2 = 0) = \Delta q \quad (q = u, d, s),$$

so that

$$G_A^{NC}(Q^2 = 0) = \frac{1}{2}(-\Delta u + \Delta d + \Delta s).$$

The difference of the up and down spin contributions, $\Delta u - \Delta d$, is proportional to the axial vector coupling constant g_A measured in hyperon β decay [7], therefore a measurement of G_A^{NC} can determine Δs .

C. Experimental measurement

The final state of an NC elastic neutrino-proton interaction consists of a neutrino and a proton. Since it isn't possible to detect the outgoing neutrino, the signal is a single proton track. In order to extrapolate the axial form factor to zero, we need to detect very low energy protons. The kinematics of the interaction are determined entirely by the proton kinetic energy, T_P ,

$$Q^2 = 2T_P M.$$

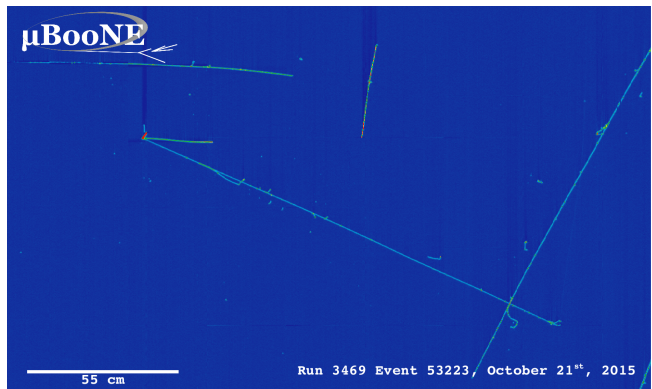


FIG. 1. A neutrino interaction in the MicroBooNE detector. This is a charged-current, muon-neutrino event with a long muon track, a charged pion track, and a short proton track coming from the interaction vertex.

Previous measurements [8–10] have been able to resolve final state protons down to a kinetic energy of $T \sim 240$ MeV which corresponds to a momentum transfer of $Q^2 = 0.45$ GeV². These measurements also found $\Delta s < 0$, but the results are highly dependent on the choice of the axial form factor Q^2 dependence. To extract Δs , G_A^s must be extrapolated to $Q^2 = 0$. Detecting events with lower momentum transfer would lessen the dependence on the choice of the model.

We estimate that MicroBooNE can detect NC elastic events down to a minimum of $Q^2 \sim 0.08$ GeV². The momentum transfer is determined by the kinetic energy of the proton in NC elastic interactions. MicroBooNE can detect protons with a track length of at least 1.5 cm which corresponds to a kinetic energy of ~ 40 MeV in liquid argon giving $Q^2 \sim 0.08$ GeV².

III. MICROBOONE

The MicroBooNE detector ?? is a liquid-argon time projection chamber (TPC) located in the Booster Neutrino Beam at Fermilab. MicroBooNE is a high-resolution detector designed to be able to accurately identify low-energy neutrino interactions. It began taking data in October of 2015. Figure 1 shows an example neutrino interaction in MicroBooNE.

A. The beam

The Booster Neutrino Beam (BNB) [11] is produced by protons from the Booster synchrotron incident on a beryllium target. The proton beam has a kinetic energy of 8 GeV, a repetition rate of 5 Hz, and an intensity of 5×10^{12} protons-per-spill. Secondary pions and kaons decay producing neutrinos with an average energy of ~ 800 MeV. The estimated BNB flux is shown in Fig. 2. MicroBooNE has received 3.6×10^{20} protons-on-target in

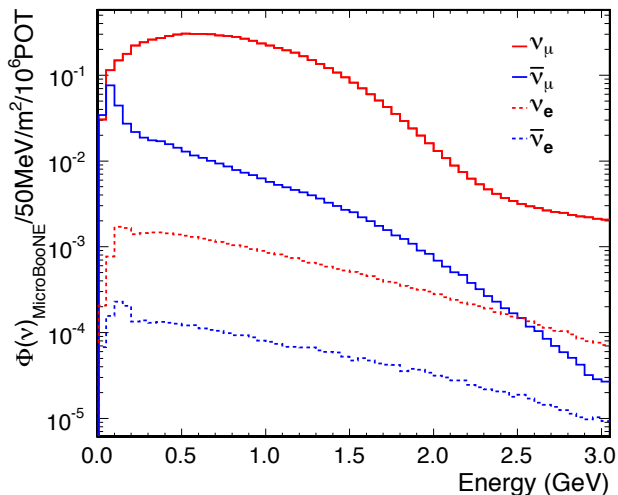


FIG. 2. The estimated Booster Neutrino Beam flux at MicroBooNE.

its first year of running.

B. The detector

The MicroBooNE TPC [12] has an active mass of 89 tons of liquid argon. It is 10 meters long in the beam direction, 2.3 meters tall, and 2.5 meters in the electron drift direction. It takes 2.3 ms for electrons to drift across the full width of the TPC at the operating electric field of 273 V/cm. Events are read out on three anode wire planes with 3 mm spacing. In addition to the TPC, there is a light collection system which consists of 32 8-inch PMTs with nanosecond timing resolution. The PMTs determine the initial time of the interaction to help with cosmic rejection. In order for an event to be read out, there must be an optical signal within a 23 μs window around the BNB spill.

C. The effect on Δs uncertainty

Global fits to electron-proton and neutrino-proton elastic scattering data have found $\Delta s = -0.30 \pm 0.42$ [13]. Based on data from a simulation of the MicroBooNE detector and the BNB beam, the uncertainty on the global fit to Δs is estimated to decrease by a factor of ten when including MicroBooNE data.

IV. AUTOMATED EVENT SELECTION

MicroBooNE is close to the surface of the Earth, which results in a large cosmic ray background. Each triggered event is read out for 4.8 ms (approximately twice the electron drift time), and there are an average of twelve cosmic muon tracks per readout frame [14]. This can be

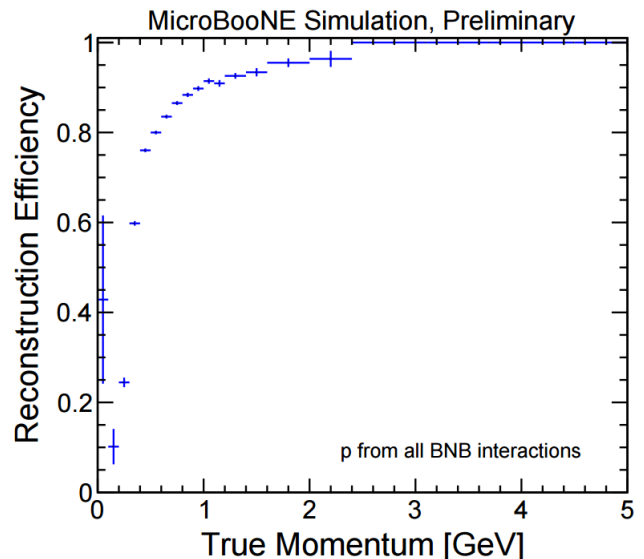


FIG. 3. Reconstruction efficiency of the Pandora algorithm for the proton with the most hits in all simulated BNB interactions, shown as a function of their true momentum [15].

seen in the bottom image in Fig. 4. In addition, there are approximately five times as many event triggers caused by cosmic rays coincident with the BNB spill than actual neutrino interactions. During MicroBooNE's three year run, we expect to have $\sim 200,000$ neutrino interactions and $\sim 1,000,000$ cosmic interactions. This means that automated neutrino event reconstruction and identification algorithms are required. These algorithms are currently being developed for liquid argon TPCs.

A. Track reconstruction in LArSoft

Track reconstruction is handled in the Liquid Argon Software framework (LArSoft) [16]. The three main stages of reconstruction in LArSoft are hit finding, track finding, and event identification.

One-dimensional hits are found by fitting Gaussian functions to noise-filtered [17] waveforms that are read out from the anode wires in the TPC. This is done for all of the wires on all three of the planes. The result is a two-dimensional image for each of the three wire planes, where the two dimensions are wire number and time. These 2D hits are used as inputs to the Pandora Software Development Kit [15]. Pandora contains pattern recognition algorithms that have been optimized to reconstruct tracks from neutrino interactions in liquid argon TPCs at the BNB energy range. The Pandora algorithms take a set of hits and reconstruct neutrino interaction vertices.

Neutral-current elastic interactions are the most difficult to detect automatically because there is only one visible particle coming from the interaction vertex. There is no unique topology separating these events from the cos-

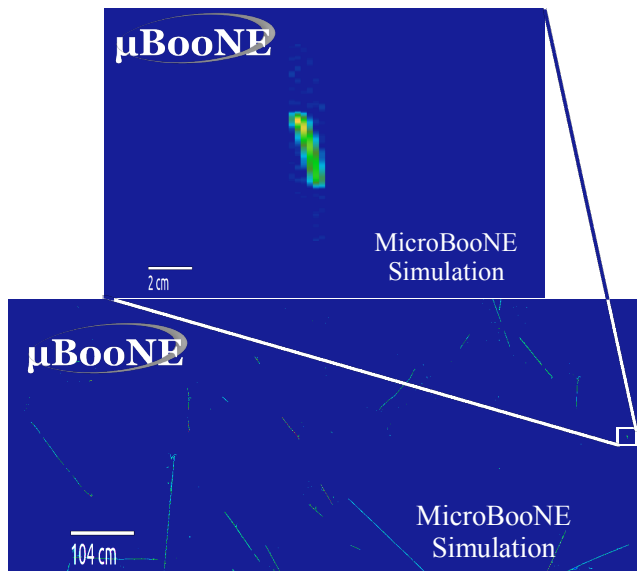


FIG. 4. 2D event display of a simulated neutral-current elastic event in MicroBooNE that was classified as a proton. The top image is a close-up event display of the simulated proton track. The bottom image shows the side view of the entire MicroBooNE TPC. All of the additional tracks are from cosmic rays.

mic background. The current reconstruction efficiency for tracks from NC elastic proton events in simulation is approximately 0.5, and this number is rapidly improving. The reconstruction efficiency for the proton with the most hits in all BNB interactions is shown as a function of simulated proton momentum in Fig. 3. Once tracks are reconstructed we attempt to identify the type of particle and interaction that produced them. In the NC elastic case, we want to specifically select proton tracks.

B. Proton track identification

1. Gradient decision tree boosting

To identify proton tracks, we use a gradient-boosted decision tree classifier. We chose to use decision trees because they are easily interpretable and the inputs can be a mix of numeric and categorical variables. Below is a short description of gradient tree boosting. A more detailed description can be found in the documentation for the XGBoost[18] software library that was used.

A decision tree can be thought of as a series of if/else statements that separate a data set into two or more classes. The goal of each cut is to increase the information gain. For numerical variables any cut value can be selected by the tree. At each node of the tree, a split is chosen to maximize information gain until a set level of separation is reached. At the terminus of the series of splits, called a leaf, a class is assigned.

Two weaknesses of decision trees are their tendency to

over fit the training data and the fact that the output is a class label and not a probability. Gradient-boosting addresses both of these issues by combining many weak classifiers into a strong one. Each weak classifier is built based on the error of the previous one. For a given training set, whenever a sample is classified incorrectly by a tree, that sample is given a higher importance when the next tree is being created. Mathematically, each tree is training on the gradient of the loss function. After all of the trees have been created, each tree is given a weight based on its ability to classify the training set, and the output of the gradient-boosted decision tree classifier is the probability that a sample is in a given class.

2. The decision tree model

We created a multi-class gradient-boosted decision tree classifier, using the XGBoost software library, to separate five different track types: any proton track, muons or pions from BNB neutrino interactions, tracks from electromagnetic showers from BNB interactions, and any non-proton track produced by a cosmic ray interaction. The classifier takes reconstructed track features as input and outputs a probability of the track having been produced by each of the given particle types. The reconstructed features are based on the track's geometric, calorimetric, and optical properties.

The training data that we use to make the decision trees comes from Monte Carlo simulation. The BNB interactions are simulated using the GENIE neutrino generator [19], and cosmic interactions are simulated using the CORSIKA cosmic ray generator [20]. The particles generated by GENIE and CORSIKA are passed to Geant4 [21] where they are propagated through a simulated MicroBooNE detector. For training and testing of the trees we only use tracks that were reconstructed in LArSoft.

Of the reconstructed test tracks that were input to the classifier, 84% of the protons from simulated neutrino interactions, and 63% of the protons from simulated cosmic interactions were classified correctly as protons. Figure 5 shows the protons from simulated neutrino interactions as a function of proton kinetic energy. Of the reconstructed test tracks that were classified as protons, 89% were true simulated protons (22% neutrino induced protons and 67% cosmic induced protons). Figure 6 shows the breakdown of track types that are classified as protons. To maximize efficiency or purity we can require a lower or higher proton probability from the classifier. Figure 7 shows the efficiency versus purity for different proton probability cuts in the range from zero to one.

The decision tree classifier was used on a small sample of MicroBooNE data as a performance check. Figures 8–10 show tracks from the data sample that were selected by the classifier as being very likely protons.

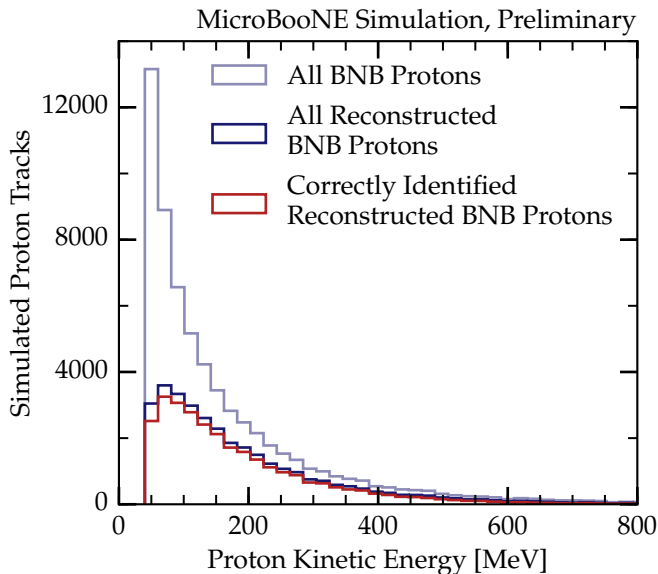


FIG. 5. Number of simulated proton tracks as a function of true simulated kinetic energy is shown. The light blue line shows the total number of protons from simulated BNB neutrino interactions. The dark blue line shows the total number of those tracks that were reconstructed with the Pandora algorithms. The red line shows the subset of the reconstructed tracks that are classified as protons by the boosted decision trees.

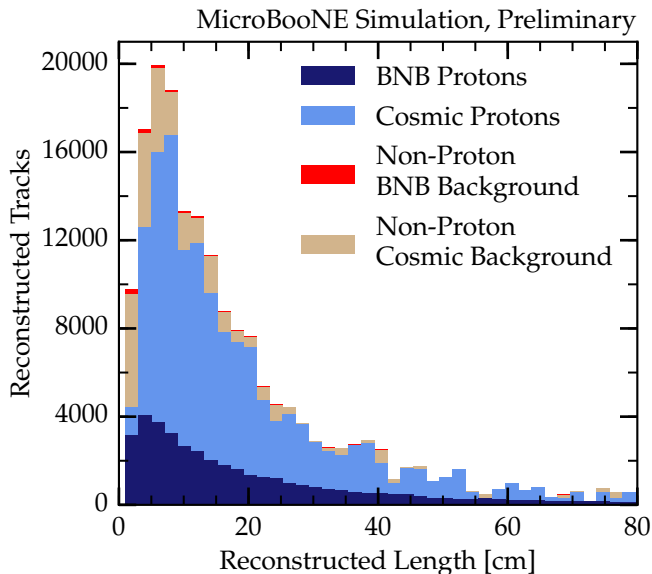


FIG. 6. Breakdown of the simulated particle types that are classified as protons by the boosted decision trees as a function of reconstructed track length. The blue filled area shows all simulated protons, both cosmic and neutrino-induced, and the dark blue line shows the protons from simulated BNB neutrino interactions. The tan filled area shows all other simulated cosmic tracks that are classified as protons, and the red filled area shows all other tracks from simulated BNB neutrino interactions that are classified as protons.

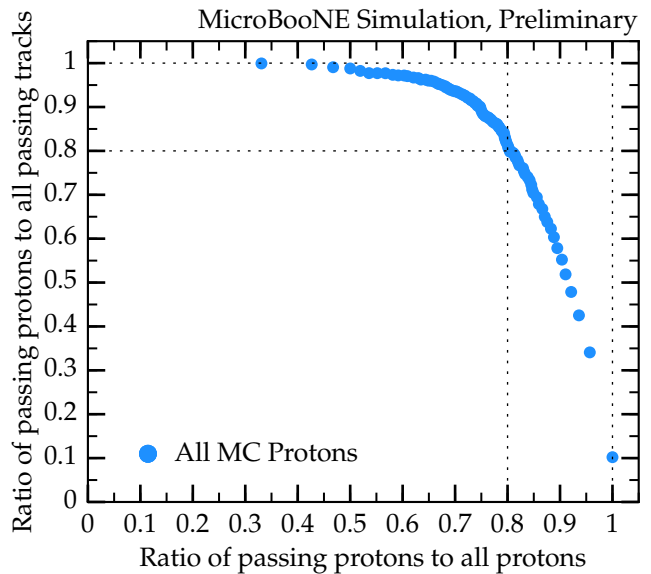


FIG. 7. The efficiency versus the purity of simulated protons selected by the boosted decision tree classifier for a series of proton probability cuts between zero and one.

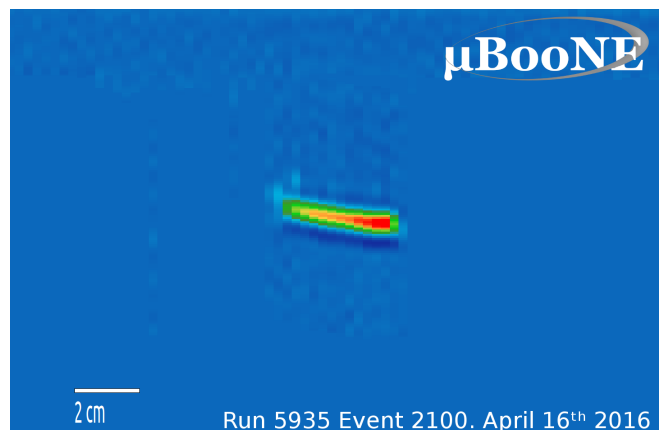


FIG. 8. Proton track candidate in MicroBooNE data. The track was selected by the decision tree classifier as being very likely a proton.

C. NC elastic event selection

So far, we have kept the proton selection general to all interaction types. For NC elastic events, we would use the output of the decision trees along with other event information such as the total number of reconstructed tracks to select the events of interest. This can also be used to select charged-current elastic events with a similar efficiency to use for normalization of the NC elastic cross section. If we are only interested in one specific topology, and do not wish to be general, it is trivial to re-train the classifier using protons from NC elastic interactions as the only positive input and protons from other interactions as a background input.



FIG. 9. Proton track candidate in MicroBooNE data. The track was selected by the decision tree classifier as being very likely a proton.

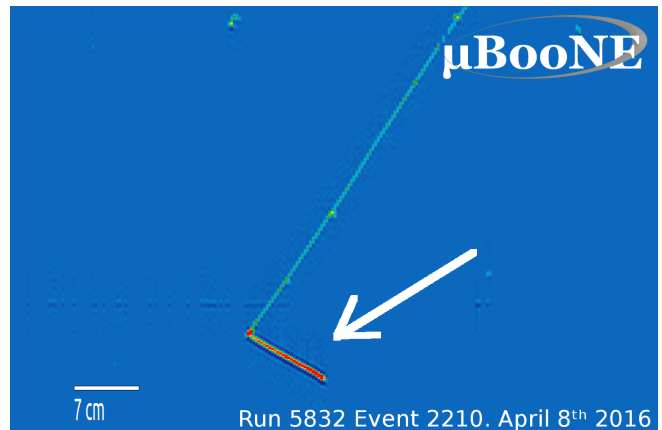


FIG. 10. Proton track candidate in MicroBooNE data. The white arrow points to a track that was selected by the decision tree classifier as being very likely a proton.

V. CONCLUSIONS

Whether the strange quarks in the nucleon sea contribute negatively or not at all to the spin of the nucleon is an open question. Elastic neutrino-proton scattering offers an unique way to determine Δ_s that is independent of the assumptions required by previous measurements. The MicroBooNE liquid argon TPC can detect low- Q^2 NC elastic events and is currently taking neutrino data at Fermilab. Automated event reconstruction and selection methods are being developed to analyze the large amount of high-resolution neutrino events in MicroBooNE.

-
- [1] W. M. Alberico, S. M. Bilenky, and C. Maieron, Phys. Rept. **358**, 227 (2002), arXiv:hep-ph/0102269 [hep-ph].
 - [2] J. Ashman *et al.* (European Muon), *Internal spin structure of the nucleon. Proceedings, Symposium, SMC Meeting, New Haven, USA, January 5-6, 1994*, Nucl. Phys. **B328**, 1 (1989).
 - [3] Ellis, John and Jaffe, Robert, Phys. Rev. D **9**, 1444 (1974).
 - [4] C. A. Aidala, S. D. Bass, D. Hasch, and G. K. Mallot, Rev. Mod. Phys. **85**, 655 (2013), arXiv:1209.2803 [hep-ph].
 - [5] D. S. Armstrong and R. D. McKeown, Ann. Rev. Nucl. Part. Sci. **62**, 337 (2012), arXiv:1207.5238 [nucl-ex].
 - [6] G. D. Cates, C. W. de Jager, S. Riordan, and B. Wojtsekhowski, Phys. Rev. Lett. **106**, 252003 (2011), arXiv:1103.1808 [nucl-ex].
 - [7] C. Patrignani *et al.* (Particle Data Group), Chin. Phys. **C40**, 100001 (2016).
 - [8] L. A. Ahrens *et al.*, Phys. Rev. **D35**, 785 (1987).
 - [9] Garvey, G. T. and Louis, W. C. and White, D. H., Phys. Rev. C **48**, 761 (1993).
 - [10] A. A. Aguilar-Arevalo *et al.* (MiniBooNE), Phys. Rev. **D82**, 092005 (2010), arXiv:1007.4730 [hep-ex].
 - [11] A. A. Aguilar-Arevalo *et al.* (MiniBooNE), Phys. Rev. **D79**, 072002 (2009), arXiv:0806.1449 [hep-ex].
 - [12] R. Acciarri *et al.* (MicroBooNE), Submitted to: JINST (2016), arXiv:1612.05824 [physics.ins-det].
 - [13] S. Pate and D. Trujillo, *Proceedings, 25th International Nuclear Physics Conference (INPC 2013): Florence, Italy, June 2-7, 2013*, EPJ Web Conf. **66**, 06018 (2014), arXiv:1308.5694 [hep-ph].
 - [14] The MicroBooNE Collaboration, MicroBooNE Public Note (2016) MICROBOONE-NOTE-1002-PUB .
 - [15] The MicroBooNE Collaboration, MicroBooNE Public Note (2016) MICROBOONE-NOTE-1015-PUB .
 - [16] E. D. Church, (2013), arXiv:1311.6774 [physics.ins-det].
 - [17] The MicroBooNE Collaboration, MicroBooNE Public Note (2016) MICROBOONE-NOTE-1009-PUB .
 - [18] Tianqi Chen and Carlos Guestrin, CoRR (2016), arXiv:1603.02754.
 - [19] C. Andreopoulos *et al.*, Nucl. Instrum. Meth. **A614**, 87 (2010), arXiv:0905.2517 [hep-ph].
 - [20] D. Heck, G. Schatz, T. Thouw, J. Knapp, and J. N. Capdevielle, (1998).
 - [21] S. Agostinelli *et al.* (GEANT4), Nucl. Instrum. Meth. **A506**, 250 (2003).